SETAC PRESS

Environmental Toxicology and Chemistry, Vol. 21, No. 3, pp. 659–671, 2002
Printed in the USA
0730-7268/02 $9.00 + .00

AgDRIFT®: A MODEL FOR ESTIMATING NEAR-FIELD SPRAY DRIFT FROM AERIAL APPLICATIONS

MILTON E. TESKE,*† SANDRA L. BIRD,‡ DAVID M. ESTERLY,§ THOMAS B. CURBISHLEY,† SCOTT L. RAY,‖ and STEVEN G. PERRY#

†Continuum Dynamics, 34 Lexington Avenue, Ewing, New Jersey 08618, USA
‡U.S. Environmental Protection Agency, 960 College Station Road, Athens, Georgia 30605
§Environmental Focus, 2801 Bexley Court, Wilmington, Delaware 19808, USA
‖Dow AgroSciences LLC, 9330 Zionsville Road, Indianapolis, Indiana 46268, USA
#Atmospheric Sciences Modeling Division, Air Resources Laboratory/NOAA (MD-20), Research Triangle Park, North Carolina 27711, USA

(*Received* 26 *September* 2000; *Accepted* 13 *August* 2001)

Abstract—The aerial spray prediction model AgDRIFT® embodies the computational engine found in the near-wake Lagrangian model AGricultural DISPersal (AGDISP) but with several important features added that improve the speed and accuracy of its predictions. This article summarizes those changes, describes the overall analytical approach to the model, and details model implementation, application, limits, and computational utilities.

Keywords—Spray model Lagrangian Drift Deposition Aerial application

INTRODUCTION

Drift of pesticides from the target site during aerial spray applications is a source of environmental concern due to its potential human health impacts, downwind contamination and damage to crops and livestock, and endangerment of ecological resources. The Spray Drift Task Force, a coalition of agricultural chemical companies, has gathered field and laboratory data based on the assumption that pesticide drift is primarily a function of environmental conditions, physical properties of the spray solution, and application equipment configuration and not of the active ingredient per se [1]. The sensitivity of drift to numerous factors, including atmospheric conditions [2–6] and application equipment [6–8], makes field testing the full range of possible meteorological and application scenarios difficult. Modeling provides a coherent framework for evaluating the potential risks of spray operations and the potential effectiveness of possible mitigation options. Both the Spray Drift Task Force and the U.S. Environmental Protection Agency's Office of Pesticide Programs strongly felt that a spray drift modeling tool supported by input databases and postprocessing toolbox utilities would improve both the efficiency and reliability of the pesticide product evaluation and registration process. AgDRIFT® (Stewart Agricultural Research Services, Macon, MO, USA) is the realization of this joint vision of a spray drift assessment tool suitable for use in the regulatory arena.

A number of models have been developed to predict the drift and deposition from aerial spray applications [9–18]. These aerial spray models fall into two general categories—empirical and mechanistic. The empirical models [9,10] do not take into account any physical basis for spray drift and are generally applicable only to situations very similar to those for which they were developed. The ideal model for evaluating off-site movement of pesticides, setting buffer zones around sensitive areas, and determining effectiveness of mitigation options needs to include mechanistic descriptions of important processes such as gravitational acceleration, air resistance, droplet evaporation, and mode of application.

Simple mechanistic models developed for evaluation of spray generally fall into two categories based on the mathematical approach to turbulent mixing, i.e., Gaussian dispersion equations and particle tracking models (Lagrangian particle trajectory) [19]. Gaussian modeling [11,14,16,17] is a classical approach used in atmospheric dispersion modeling of releases from tall stacks and line, area, and volume sources and is well suited for modeling moderately long-range drift (0.5–10 km) and simulating the effects of atmospheric stability. However, the Gaussian approach does not provide much resolution in the representation of equipment and near-field dynamics in the flow field near the aircraft. Lagrangian models [12,15,18], on the other hand, track a cohort of droplets in a given drop size category and overlay a random component on the movement of the droplets to account for atmospheric turbulence. The Lagrangian approach lends itself to detailed modeling of the effects of application equipment on spray dispersal and thus, as an approach, most effectively meets the needs for a regulatory assessment tool that can be used to evaluate the mitigating effects of alternative equipment uses and near-field buffer zones.

The real power of the model presented here lies in its relative simplicity. AgDRIFT does not employ a full-physics Navier–Stokes approach but instead incorporates a much simpler method that yields high correlations with observed deposition. This simplicity is very desirable in a regulatory context and lends itself to wide use and consistent results.

The AGDISP model [12] forms the computational engine of AgDRIFT. The AGDISP is based on a Lagrangian approach to the solution of the spray material equations of motion and includes simplified models for the effects of the aircraft wake and aircraft-generated and ambient turbulence. Reed [20] first developed the equations of motion for spray material released

* To whom correspondence may be addressed (milt@continuum-dynamics.com).

from nozzles on an aircraft. His insight was the realization that the wingtip vortices play a significant role in the subsequent behavior of the spray material released close to the aircraft. Vortex swirling behavior can be quantified by a simple model that, when combined with the local wind speed and gravity, effectively predicts the motion of spray material released into it. Other researchers expanded on this approach to produce more detailed models of the problem [15,21–24]. The original AGDISP model built upon these studies but included the innovative step of developing ensemble-averaged turbulence equations to predict the growth of the spray cloud during the calculations, eliminating the need for a random component in the solution procedure.

The AGDISP has an extensive history of use and development by several federal agencies. The initial computational approach for AGDISP was defined under a 1979 grant by the National Aeronautics and Space Administration to develop and demonstrate a particle dispersion computer code that models deposition on a horizontal surface. Over nearly 20 years, with continuing support from the U.S. Department of Agriculture Forest Service and the U.S. Army, AGDISP was developed [25] and refined, both as a stand-alone code [12] and as the near-wake model in Forest Service Cramer–Barry–Grim (FSCBG) [14]. In this same time period, considerable effort has been made toward understanding the spray application problem. This improved understanding has led to extensive data assembly efforts to facilitate use of the model, including collecting specifications for most of the aircraft used in aerial spraying in the United States [26] and testing the sensitivity of deposition to aircraft type [27], collecting drop size distributions of agricultural products in use today [28,29] and investigating their effect on deposition [8] and our ability to model atomization [30–33], performing an extensive series of sensitivity studies of the influence of all inputs into the model [34–38] in an effort to clarify which variables influence field applications, and evaluating model performance on available field data sets [39].

AgDRIFT is a Microsoft® Windows™ (Redmond, WA, USA)-based implementation of the AGDISP program aimed at addressing the assessment of off-site drift of pesticide from agricultural applications. It contains aerial, ground, and orchard/airblast models. The initial focus and original applications of AGDISP were primarily toward defining in-swath deposition patterns or as a near-wake model for forestry or other high-release applications where calculations for downwind deposition were made following a hand-off from the Lagrangian calculations to a Gaussian plume algorithm [14]. The use of AgDRIFT as a tool for assessing off-field drift and mitigation of drift from low-flight applications for regulatory decision-making required minor computational modifications to the original AGDISP model, implementation of data libraries, and model evaluation in this type of application.

This article is the second in a series of three articles. The first [1] describes a series of aerial application field studies measuring off-site drift and deposition of pesticides and wind tunnel drop size distribution measurements, which were used in the third article [40] to evaluate the performance of AgDRIFT for low-flight agricultural applications. The objective of the present article is to present an up-to-date description of the computational algorithms implemented in AgDRIFT and to provide an overview of their application in this tool designed for use in regulatory assessments.

MODEL FORMULATION

Spray material released from an aircraft is usually modeled as a discrete set of droplets, collected into categories and called a drop size distribution. Each drop size category is defined by its volume average diameter and volume fraction (the total volume fraction of the released spray material is 1.0) and is examined sequentially by the model. A Lagrangian approach is used to develop the equations of motion for discrete droplets released from the aircraft, with the resulting set of ordinary differential equations solved exactly from time step to time step. Drop flight path as a function of time after release is computed as the mean droplet locations X_i for all droplets included in the simulation. The positive X direction is taken as the direction from which the aircraft is flying, the Y direction is off the right wing as viewed from the pilot's seat, and the Z direction is vertical upward. The interaction of the released material with the turbulence in the environment creates turbulent correlation functions for droplet position and velocity $\langle x_i v_i \rangle$, for velocity variance $\langle v_i v_i \rangle$, and for position variance $\langle x_i x_i \rangle$, where x_i is the fluctuating droplet position, v_i is the fluctuating droplet velocity, and $\langle\rangle$ denotes ensemble average. The square root of $\langle x_i x_i \rangle$ gives the standard deviation σ of the droplet motion about the mean described by X_i.

The novel feature of the AGDISP (and AgDRIFT) methodology is that the dispersion of a group of similarly sized droplets (contained within each drop size category), resulting from turbulent fluid fluctuations in the atmosphere, is quantitatively computed within the wake of the aircraft as the group of droplets descends toward the surface. The Lagrangian equations governing the behavior of a droplet in motion may be written

$$\frac{d^2}{dt^2}(X_i + x_i) = [U_i + u_i - V_i - v_i]\left[\frac{1}{\tau_p}\right] + g_i \qquad (1)$$

$$\frac{d}{dt}(X_i + x_i) = V_i + v_i \qquad (2)$$

where t is time, U_i is the mean local velocity, u_i is the fluctuating local velocity, V_i is the mean droplet velocity, v_i is the fluctuating droplet velocity, g_i is gravity (0, 0, $-g$), and the drag force on the droplet is represented by the droplet relaxation time

$$\tau_p = \frac{4}{3}\frac{D\rho}{C_D \rho_a |U_i - V_i|} \qquad (3)$$

where D is the droplet diameter, ρ is the droplet density, C_D is the droplet drag coefficient, and ρ_a is the air density. Here, the position and velocity vectors are written in tensor notation as the sum of an ensemble averaged mean (upper case) and fluctuating components about the mean (lower case). The term representing the effect of evaporation on droplet acceleration has been removed from Equation 1 because its effect is small and its presence significantly complicates the problem (and makes the later analytical solution to Equations 1 and 2 impossible). The C_D is evaluated empirically for spherical droplets as [41]

$$C_D = \frac{24}{\mathrm{Re}}[1 + 0.197\mathrm{Re}^{0.63} + 0.00026\mathrm{Re}^{1.38}] \qquad (4)$$

where

$$\mathrm{Re} = \frac{\rho_a D |U_i - V_i|}{\mu_a} \qquad (5)$$

is the Reynolds number and μ_a is the air viscosity. The relaxation time τ_p, defined in Equation 3, has physical significance with regard to dispersion in that it is the *e*-folding time required for a droplet to catch up to its local velocity (for V_i to approach U_i). If Equations 1 and 2 are ensemble averaged, we obtain

$$\frac{d^2X_i}{dt^2} = [U_i - V_i]\left[\frac{1}{\tau_p}\right] + g_i \quad (6)$$

$$\frac{dX_i}{dt} = V_i \quad (7)$$

Equations 6 and 7 were first examined by Reed [20] and, with a specification of the local velocity field U_i, can be solved to obtain the mean trajectory paths for the spray material issuing from each nozzle. Reed assumed that the local velocity field was generated by a counter-rotating pair of vortices positioned at the aircraft wing tips. This velocity field provides most of the velocity effects close to the aircraft and will be described later, although not in the form he suggested.

Substituting Equation 6 into Equation 1 and Equation 7 into Equation 2, results in the fluctuation equations, which may be premultiplied by x_i and v_i, ensemble averaged, and manipulated to yield

$$\frac{d}{dt}\langle x_i x_i\rangle = 2\langle x_i v_i\rangle \quad (8)$$

$$\frac{d}{dt}\langle x_i v_i\rangle = [\langle x_i u_i\rangle - \langle x_i v_i\rangle]\left[\frac{1}{\tau_p}\right] + \langle v_i v_i\rangle \quad (9)$$

$$\frac{d}{dt}\langle v_i v_i\rangle = 2[\langle u_i v_i\rangle - \langle v_i v_i\rangle]\left[\frac{1}{\tau_p}\right] \quad (10)$$

where the i indices are now not summed. Equation 8 represents the growth of the spray cloud, as $\langle x_i x_i\rangle$ is the position variance around the mean droplet location X_i. Equations 8 to 10 require the specification of $\langle x_i u_i\rangle$ and $\langle u_i v_i\rangle$, correlations of the droplet position and velocity with the local background velocity, respectively, before solution is possible.

These correlations are developed by assuming that the fluctuating local velocity may be represented by its Fourier transform $\hat{u}_i(\omega)$,

$$u_i = \frac{1}{2\pi}\int_{-\infty}^{\infty} \hat{u}_i(\omega)e^{i\omega t}\, d\omega \quad (11)$$

where ω is frequency, and solving the fluctuating equations

$$\frac{d^2x_i}{dt^2} = [u_i - v_i]\left[\frac{1}{\tau_p}\right] \quad (12)$$

$$\frac{dx_i}{dt} = v_i \quad (13)$$

to obtain solutions for x_i and v_i of the form

$$x_i = \frac{1}{2\pi}\int_{-\infty}^{\infty} \hat{u}_i(\omega)\left[\frac{e^{i\omega t} - 1 + i\omega\tau_p(e^{-t/\tau_p} - 1)}{i\omega(1 + i\omega\tau_p)}\right] d\omega \quad (14)$$

$$v_i = \frac{1}{2\pi}\int_{-\infty}^{\infty} \hat{u}_i(\omega)\left[\frac{e^{i\omega t} - e^{-t/\tau_p}}{1 + i\omega\tau_p}\right] d\omega \quad (15)$$

for constant initial conditions. Upon multiplying these results by u_i and ensemble averaging (with Parseval's theorem), equations are obtained for the needed correlations

$$\langle x_i u_i\rangle = \int_{-\infty}^{\infty} \Phi_u(\omega)\left[\frac{\sin\omega t}{\omega} - \frac{\tau_p}{1 + \tau_p^2\omega^2} \times (1 - e^{-t/\tau_p}\cos\omega t + \tau_p\omega e^{-t/\tau_p}\sin\omega t)\right] d\omega \quad (16)$$

$$\langle u_i v_i\rangle = \int_{-\infty}^{\infty} \Phi_u(\omega)\frac{1}{1 + \tau_p^2\omega^2} \times [1 - e^{-t/\tau_p}\cos\omega t + \tau_p\omega e^{-t/\tau_p}\sin\omega t]\, d\omega \quad (17)$$

where $\Phi_u(\omega)$ is the Lagrangian spectral density function. As noted in [42], in stationary turbulence, the variance $\langle x_i x_i\rangle$ can be expressed in terms of an integral of the Lagrangian autocorrelation coefficient. In AgDRIFT, the transform of this function is approximated by

$$\Phi_u(\omega) = \frac{1}{3\pi}\frac{\Lambda}{U}q^2\frac{1 + 3(\omega\Lambda/U)^2}{[1 + (\omega\Lambda/U)^2]^2} \quad (18)$$

where Λ is the integral scale of the mean square turbulence level q^2 and U is the free stream velocity [43,44]. The spectral density function assumed here approximates the turbulence found in an aircraft wake, where U is interpreted as the relative velocity $|U_i - V_i|$, thereby permitting us to integrate the equations analytically to find

$$\langle x_i u_i\rangle = \frac{q^2}{3}\left[-\tau_p K_1 + \tau_p\left(K_2 - \frac{\tau_p}{\tau_t}K_3\right)e^{-t/\tau_p} + \tau_t K_4\right] \quad (19)$$

$$\langle u_i v_i\rangle = \frac{q^2}{3}\left[K_1 - \left(K_2 - \frac{\tau_p}{\tau_t}K_3\right)e^{-t/\tau_p}\right] \quad (20)$$

where

$$K_1 = \frac{1}{2}\frac{\left[3 - \left(\frac{\tau_p}{\tau_t}\right)^2\right]\left[1 - \frac{\tau_p}{\tau_t}\right] + \left(\frac{\tau_p}{\tau_t}\right)^2 - 1}{\left[1 - \left(\frac{\tau_p}{\tau_t}\right)^2\right]^2} \quad (21)$$

$$K_2 = \frac{1}{2}\frac{\left[3 - \left(\frac{\tau_p}{\tau_t}\right)^2\right]\left[e^{-t/\tau_t} - \frac{\tau_p}{\tau_t}e^{-t/\tau_p}\right] + \left[\left(\frac{\tau_p}{\tau_t}\right)^2 - 1\right]\left[1 + \frac{t}{\tau_t}\right]e^{-t/\tau_t}}{\left[1 - \left(\frac{\tau_p}{\tau_t}\right)^2\right]^2} \quad (22)$$

$$K_3 = \frac{1}{2}\frac{\left[3 - \left(\frac{\tau_p}{\tau_t}\right)^2\right][e^{-t/\tau_t} - e^{-t/\tau_p}] + \left[\left(\frac{\tau_p}{\tau_t}\right)^2 - 1\right]\frac{t}{\tau_t}e^{-t/\tau_t}}{\left[1 - \left(\frac{\tau_p}{\tau_t}\right)^2\right]^2} \quad (23)$$

$$K_4 = \frac{1}{2}\left[1 + e^{-t/\tau_t}\left(\frac{t}{\tau_t} - 1\right)\right] \quad \text{and} \quad (24)$$

$$\tau_t = \frac{\Lambda}{|U_i - V_i| + \frac{3}{8}q} \quad (25)$$

is the travel time of the droplet through a turbulent eddy of scale length Λ. Equation 25 recovers the proper limit for $V_i \rightarrow U_i$ [45].

Equations 6 to 10 are therefore governed by two time scales: τ_p and τ_t. Their consistent limiting behavior is of interest here: as τ_p approaches zero (drop size approaches zero), the droplet

will follow the fluctuations in the flow field, and these equations may be solved to yield

$$\langle x_i x_i \rangle = \frac{q^2}{3}\tau_t t = \frac{8}{9}q\Lambda t \tag{26}$$

recovering the well-known large-time result that the position variance grows as the product of the turbulence level q and time [46]; and as τ_p approaches infinity (drop size becomes massive), the droplets move independently of the flow field, and these same equations may be solved in this limit to yield

$$\langle x_i x_i \rangle = \frac{q^2}{3}\left(\frac{\tau_t}{\tau_p}\right)^3 t^2 \tag{27}$$

where the time-squared behavior is now consistent with the short-time result (again found in [46]). As τ_p reaches infinity in this limit, the variance remains zero since the droplets are too massive to be dispersed by turbulent fluctuations.

With the position and velocity information available for the droplet at any time during the simulation, Equations 6 to 10 may be integrated exactly as an initial-value problem for the solution at the next time step, with the assumption that the background conditions U_i, $\langle x_i u_i \rangle$, and $\langle u_i v_i \rangle$ are constant across each time step. For example, the solution to the mean equations becomes

$$X_i = X_0 - \tau_p[U_i - V_0 + g_i\tau_p][1 - e^{-\Delta t/\tau_p}] + [U_i + g_i\tau_p]\Delta t \tag{28}$$

$$V_i = -\tau_p[U_i - V_0 + g_i\tau_p]e^{-\Delta t/\tau_p} + U_i + g_i\tau_p \tag{29}$$

where X_o is the initial droplet position at the beginning of the time step Δt and V_o is the initial droplet velocity at the beginning of the time step. The turbulent correlations are solved in a similar manner but are not shown here because of their complexity.

Evaporation modeling

The evaporation model in AgDRIFT is based on the *D*-squared law as suggested in [22], in which the time rate of change of drop diameter is taken as

$$\frac{dD}{dt} = -\frac{D}{2\tau_e\left(1 - \frac{t}{\tau_e}\right)} \tag{30}$$

where

$$\tau_e = \frac{D^2}{84.76\Delta\Theta(1 + 0.27\mathrm{Re}^{1/2})} \tag{31}$$

is the evaporation time scale of the droplet and the wet bulb temperature depression $\Delta\Theta = \Theta_d - \Theta_w$ is evaluated from the Carrier equation [47]

$$p_s = p_w - \frac{(p_b - p_w)(\Theta_d - \Theta_w)}{1{,}555.6 - 0.7\Theta_w} \tag{32}$$

where p_s is the pressure of water vapor in the atmosphere, p_w is the pressure of saturated water vapor at the wet bulb temperature, p_b is the barometric pressure, Θ_d is the dry bulb temperature, and Θ_w is the wet bulb temperature. The water vapor pressure is found from the simple expression $p_s = 0.01\phi p_d$, where ϕ is the relative humidity (in percent) and p_d is the pressure of saturated water vapor at the dry bulb temperature. Because the pressures p_d and p_w are related to their corresponding temperatures Θ_d and Θ_w through the saturation line in the steam tables [48], the solution to Equation 32 can be performed only by iteration. The saturation line in the steam tables may be expressed as

$$\beta = \exp\left[\frac{1}{\Theta}\frac{\sum_{n=1}^{5} k_n(1 - \Theta)^n}{1 + k_6(1 - \Theta) + k_7(1 - \Theta)^2} - \frac{(1 - \Theta)}{k_8(1 - \Theta)^2 + k_9}\right] \tag{33}$$

where β is the pressure divided by the critical pressure, Θ is the absolute temperature divided by the critical temperature, and k_n are curve-fitting constants to the saturation line ($k_1 = -7.691234564$, $k_2 = -26.08023696$, $k_3 = -168.1706546$, $k_4 = 64.23285504$, $k_5 = -118.9646225$, $k_6 = 4.167117320$, $k_7 = 20.97506760$, $k_8 = 1{,}000{,}000{,}000.0$, $k_9 = 6.0$). Recent research [49,50] supports the assumption that aerially applied agricultural materials (in water-based carriers) show evaporative characteristics similar to water. For water [22], a suggested evaporation rate of $\lambda_\infty = 84.76\ \mu m^2/(s\cdot°C)$ as shown in Equation 31. This value may be obtained from an expression developed for quiescent flow [51],

$$\lambda = \frac{8\kappa}{\rho L} \tag{34}$$

where κ is the thermal conductivity of air and L is the latent heat of vaporization. Tests by the Spray Drift Task Force showed that the evaporation rate—with flow over the droplet—could be somewhat lower, down to $\lambda_\infty = 70.24\ \mu m^2/(s\cdot°C)$ for deionized water, well within a 10 to 15% variation in the evaluation of thermal conductivity and latent heat [52], and that the evaporation rate is further reduced as the relative velocity $|U_i - V_i|$ approaches zero [53]. This study set a bounding curve to λ_∞ of the form

$$\lambda/\lambda_\infty = 0.4 + 0.116\ \mathrm{Re} \tag{35}$$

This correction runs counter to scaling laws based on the Sherwood number ($\mathrm{Sh} = 1 + 0.27\ \mathrm{Re}^{1/2}$ as shown in Eqn. 31) but, when implemented into AgDRIFT, reduces downwind deposition by a factor of two and brings model predictions closer to field data measurements. With a reduced evaporation rate, drop sizes remain larger and are more likely to deposit closer to the spray block than droplets that experience higher evaporation rates.

Flow field modeling

The behavior of the released droplets is intimately connected to the local background mean velocity U_i and turbulence field q^2 through which the spray material is transported. In the Lagrangian formulation, these local effects must be approximated by models for the aircraft and the atmosphere. AgDRIFT contains a number of simplified models for the flow field velocity and turbulence levels behind aircraft.

Fixed-wing rolled-up tip vortices. When an aircraft flies at a constant altitude and speed, the aerodynamic lift generated by the lifting surfaces of the aircraft equals the aircraft weight. The majority of the lift is carried by the wings and generates one or more pairs of swirling masses of air (vortices) downstream of the aircraft [54]. If the roll up of this trailing vorticity can be approximated as occurring immediately downstream of the wing, then the mean velocity field that results may be given by known aircraft characteristics and the wing load distribu-

tion. The simplest conceptualization of a wake behind an aircraft arises when the load distribution across a wing is taken as uniform. Unfortunately, such a distribution is impossible to achieve in practice and is in fact very undesirable from an aerodynamic efficiency point of view [55]. From a practical point of view, most aircraft wings are designed to approximate an elliptical span load distribution of the form

$$\frac{\Gamma}{\Gamma_0} = \sqrt{1 - \left(\frac{y}{s}\right)^2} \tag{36}$$

where Γ is the vortex circulation strength, Γ_0 is the aircraft centerline vortex circulation strength, y is the lateral distance from the aircraft centerline, and s is the aircraft semispan. This distribution results in the most efficient means of generating lift while minimizing drag [56]. The velocity field behind the trailing edge of the wing and between the two vortices, is uniform downward. The centers of the fully rolled-up vorticity are located a distance of $\pi s/4$ along either wing. If spray material were released uniformly along the trailing edge of a wing, a prediction of the deposition of material would show a greater spread for calculations based on the uniform load wake model when compared with the elliptical load wake model. Use of an elliptically loaded wing approximation enhances the near spray block deposition pattern and diminishes the driftable fraction, both effects of which improve AgDRIFT predictions when compared with data.

With an elliptically loaded wing, the strength of each wing tip vortex is computed from the equation

$$\Gamma = \frac{2}{\pi}\frac{W}{\rho_a s U_\infty} \tag{37}$$

where W is the aircraft weight and U_∞ is the aircraft speed. The local swirl velocity V_s around each vortex may then be approximated by

$$V_s = \frac{\Gamma}{2\pi}\frac{r}{(r + r_c)^2} \tag{38}$$

where r is the distance from the vortex center to the droplet and r_c is the vortex core radius. The integral scale of turbulence is set to $\Lambda = 0.6r$ [57]. For a vortex pair, the superimposed effects of four vortices are used to simulate the overall proximity to the ground, with image vortices maintaining the no-flow inviscid ground condition. The vortex strength Γ decays with time because of atmospheric turbulence, following a simple decay model,

$$\Gamma = \Gamma_i \exp\left(-\frac{bqt}{s}\right) \tag{39}$$

where Γ_i is the initial vortex circulation strength and exp is the exponential function. This functional dependence was validated in a series of aircraft flyovers past instrumented towers [58], with an average value of $bq = 0.56$ m/s. This effect diffuses the vortex strength and permits earlier deposition downwind of the spray lines.

Helicopter in forward flight. The helicopter model partitions the helicopter weight between hover downwash and rotor tip vortices as a function of time. The hover downwash model is taken from actuator disk theory for a propeller [59] and may be written as

$$w_d = \frac{1}{R}\sqrt{\frac{FW}{2\pi\rho_a}} \tag{40}$$

where w_d is the downwash velocity at the helicopter rotor plane and R is the rotor radius of the helicopter. The strength of the vortex pair may be found from

$$\Gamma = \frac{2(1 - F)W}{\pi\rho_a R U_\infty} \tag{41}$$

where $F = \exp(-x/s)$ found by matching the behavior of this simple model with detailed helicopter models [60] as a function of the axial distance x. At the beginning of the calculation, $x = 0$, $F = 0$, and all of the weight of the helicopter provides downwash through the helicopter rotor blades. As the calculation proceeds, $x > 0$, $F \to 0$, and all of the weight transitions to provide vortex motion identical to that of a fixed-wing aircraft. Because of the exponential decay, the transition between downwash and vortex motion occurs within two rotor diameters behind the helicopter.

Spray material released ahead of the helicopter (spray boom forward) is assumed to encounter a streamline pattern similar to flow around a circular cylinder [56],

$$U = U_\infty\left(1 - \frac{R^2}{r^2} + \frac{2R^2y^2}{r^4}\right) \tag{42}$$

$$V = \frac{2U_\infty R^2 xy}{r^4} \tag{43}$$

for the free stream velocity U and lateral velocity V, until the spray material crosses the plane of the helicopter shaft centerline.

Propeller. The propeller is also modeled as an actuator disk, where the incremental velocity ΔU over the flight speed U_∞ is related to the actual thrust produced by the propeller,

$$T = 2\pi\rho_a R^2 \Delta U(U_\infty + \Delta U) \tag{44}$$

where R is now the radius of the propeller. In steady flight, the thrust equals the aircraft drag, so that

$$T = C_D\frac{1}{2}\rho_a U_\infty^2 S \tag{45}$$

where C_D is now the drag coefficient of the aircraft and S is the aircraft wing planform area. Combining Equations 44 and 45 to eliminate thrust, we obtain

$$\frac{\Delta U}{U_\infty} = \frac{1}{2}\left(-1 + \sqrt{1 + \frac{C_D S}{\pi R^2}}\right) \tag{46}$$

The effective thrust level for the propeller may be obtained as [61]

$$T = 2.5275\rho_a R^2 \Delta U^2 \tag{47}$$

and is used to generate the axial and radial velocities, u_{axial} and v_{radial}, respectively, as

$$u_{axial} = \frac{3}{8\pi}\frac{\sqrt{\frac{T}{\rho_a}}}{\epsilon x}\frac{1}{\left(1 + \frac{\eta^2}{4}\right)^2} \tag{48}$$

$$v_{radial} = \frac{1}{4}\sqrt{\frac{3}{\pi}}\frac{\sqrt{\frac{T}{\rho_a}}}{x}\frac{\left(\eta - \frac{\eta^3}{4}\right)}{\left(1 + \frac{\eta^2}{4}\right)^2} \tag{49}$$

with

$$\eta = \frac{1}{4}\sqrt{\frac{3}{\pi}}\frac{\sqrt{\frac{T}{\rho_a}}}{\epsilon}\frac{r}{x} \quad (50)$$

$$\epsilon = 0.0161\sqrt{\frac{T}{\rho_a}} \quad (51)$$

$$q^2_{prop} = 0.2034u^2_{axial} \quad (52)$$

where r is now the radius from the center of the propeller. The proportionality constant in the equation for q^2_{prop} is determined from the centerline decay of turbulence in a free jet [62].

The swirl velocity generated by the propeller is assumed to be linear out to R and then zero for larger values of r. The resulting integration yields

$$V_{tip} = \frac{U^3_\infty C_D S}{\pi\zeta\Omega R^3(U_\infty + \Delta U)} \quad (53)$$

where ζ is the propeller efficiency and Ω is the propeller rotation rate.

Mean crosswind. In a neutral atmospheric surface layer, the lateral velocity V is assumed to follow a logarithmic profile,

$$V = V_r\frac{\ln(z/z_0)}{\ln(z_r/z_0)} \quad (54)$$

where V_r is the lateral velocity at the reference height z_r, z is vertical distance, and z_0 is surface roughness. With a linear integral scale of turbulence ($\Lambda = 0.65z$), the turbulence level [63,64] becomes

$$q^2_{wind} = 0.845\left[\frac{V_r}{\ln(z_r/z_0)}\right]^2 \quad (55)$$

Flow effects are additive from all of these contributions to assemble the local velocity U_i and turbulence q at the spatial position of the droplet being examined. The solution to the Lagrangian equations of motion may therefore be undertaken. Droplet trajectories are followed from their release points at the nozzle locations until they deposit on the surface or move beyond a downwind location where they are no longer of interest.

Deposition modeling

As released spray material approaches the ground, deposition begins and continues until all unevaporated material is deposited (capture is assumed to be 100% efficient). Ground deposition is computed by assuming that the concentration of material around the mean may be taken as Gaussian,

$$C = \frac{1}{2\pi\sigma^2}\exp\left[-\frac{(y - Y)^2}{2\sigma^2}\right]\exp\left[-\frac{(z - Z)^2}{2\sigma^2}\right] \quad (56)$$

where the released spray material is at position (Y, Z). When the unevaporated material deposits as it approaches the surface, Equation 56 is integrated from far below the surface to the ground to give

$$M = \frac{1}{2\sqrt{2\pi}\sigma}\exp\left[-\frac{(y - Y)^2}{2\sigma^2}\right]\mathrm{erfc}\left(\frac{Z}{\sqrt{2}\sigma}\right) \quad (57)$$

where erfc is the complementary error function. Deposition to the ground is estimated by summing all incremental contributions to M as integration proceeds, then correcting the integrated deposition so that conservation of the released nonvolatile spray material is achieved. It may be seen that, for material falling vertically toward the surface, the pattern of chemical deposition to the ground generated by Equation 57 will be identical to the traditional Gaussian deposition.

The deposition equation requires the incremental summing of deposition as the calculation proceeds. While the trajectory analysis accurately predicts the position of each droplet, the deposition is found discretely. Thus, without any specific restrictions, the mass deposition on the ground will not generally be conserved. To guarantee conservation, the accurate sum of all droplets hitting the ground (known from the trajectory analysis) generates the exact amount of nonvolatile material that should be on the ground. This amount is compared with the incremental sum, and the incremental sum is corrected appropriately.

Stream modeling

The AgDRIFT model includes the ability to specify the location of a stream downwind of the spray block. Any ground deposition occurring across the width of the stream is assumed to enter the stream and contribute to the initial concentration of spray material in the stream. By forming an equation for the behavior of this concentration, including the effects of the stream flow rate, we may determine the dilution of the initial concentration in time and distance downstream and make an assessment of the subsequent effects on concentration.

The stream assessment solution is obtained from the exact solution to a one-dimensional, unsteady advection–diffusion equation of the form

$$\frac{\partial C_s}{\partial t} + U_s\frac{\partial C_s}{\partial x_s} = D_s\frac{\partial^2 C_s}{\partial x_s^2} - nC_s \quad (58)$$

where C_s is the stream concentration, U_s is the average stream flow speed, x_s is downstream distance, D_s is the dispersion coefficient, and n is the decay rate of the active ingredient in the deposited spray material. The dispersion coefficient may be interpreted as [65]

$$D_s = \frac{0.11U_s w^2}{d} \quad (59)$$

where w is the average stream width and d is its average depth. The stream is assumed to flow parallel to the flight lines of the aircraft (for the initial loading of the stream only) and be located at a lateral distance Y downwind of the most downwind flight line. Rapid (instantaneous) mixing is assumed to occur across the assumed rectangular cross-section of the stream when recovering the initial concentration.

The solution begins with an initial top-hat concentration from the aerial spray (whose length is the length of the flight lines) on a flight-line by flight-line basis and is integrated across the time and distance specified by the user until the concentration reaches a low value. The solution for each flight line is the product of the exact solution to Equation 58 [66] and an exponential term representing in situ decay and is of the form

$$C_s = \frac{C_i}{2}\left[\mathrm{erf}\left(\frac{a - y_s}{2\sqrt{D_s t}}\right) + \mathrm{erf}\left(\frac{a + y_s}{2\sqrt{D_s t}}\right)\right]\exp(-nt) \quad (60)$$

where C_i is the initial stream concentration, a is one half of the spray block length, $y_s = x_s - U_s t$, and erf is the error function. The most downwind flight line is assumed to deposit to the stream at $t = 0$. Each upwind flight line deposits to the stream at uniformly increasing increments in time. Solution details may be found in Teske [67].

MODEL IMPROVEMENTS

The original presentation of the AGDISP model [12] has been extended within the AgDRIFT framework to include several improvements to the accuracy of predictions of downwind drift and deposition. These improvements include a more physically correct approximation of the fully rolled-up wingtip vortices as generated from an elliptically loaded wing [55] and experimental recovery of aircraft vortex decay by local turbulence [58]; modification of the helicopter wake model to more nearly approximate the predictions from state-of-the-art wake models [60,68]; inclusion of smaller drop sizes in the drop size distribution, specifically extending the minimum size class examined to 10 μm or less, and splitting the drop size distribution (typically contained in 32 size categories) into size classes that each contain no more than 2% of the total volume fraction [13,69]; evaporation rates for typical agricultural tank mixes and the importance of the nonvolatile fraction [49,50,52]; reduction in evaporation rate at low relative wind speeds [53]; and a significant solution speed increase, incorporating an exact solution to the equations of motion on a step-by-step basis and an in-memory computation of the smoothed downwind deposition pattern.

These extensions to the aircraft wake model, the drop size distribution representation, and the evaporation model are now considered essential to the success of any model in accurately predicting downwind drift. In addition, the solution speed increase enables AgDRIFT to run rapidly in the 32-bit Windows™ (Microsoft) environment.

MODEL INPUTS

To make an accurate prediction of downwind drift and deposition, AgDRIFT requires a consistent set of inputs representing the aircraft and its flight condition, the nozzles and the drop size distributions they create, the spray material properties, and the ambient meteorology. These inputs drive the various elements of the model used to approximate the physics within the wake behind the spray aircraft and in the local environment. In general, these inputs are evaluated from the open literature (or recovered from the available model libraries), are measured during a field trial or in the laboratory or wind tunnel, or are estimated as a worst case scenario in the application of the spray product.

The complete list of inputs needed to run AgDRIFT is given in Appendix 1. Within this list are identified several broad areas of classification relating to a description of the aircraft and its power plant (rotor or propeller), the nozzles on the spray boom and the drop size distribution they create, spray material details, ambient meteorology, and other needed field information.

Aircraft characteristics include the fixed-wing semispan (or helicopter rotor radius), typical flight speed during spraying, weight, and helicopter rotor RPM. These characteristics have been collected for many agricultural aircraft in the AgDRIFT aircraft library [26,70].

Engine characteristics (for propeller-driven aircraft) include the aircraft drag coefficient, planform area, engine efficiency, propeller RPM, propeller blade radius, and spatial location of the blade hub relative to the tip of the trailing edge of the wing. These characteristics have been collected in the AgDRIFT aircraft library as well. Aircraft drag coefficient and engine efficiency have been taken as 0.1 and 0.8, respectively [12].

Nozzle characteristics include the spatial location of the spray boom relative to the centerline of the aircraft and the vertical distance to the tip of the trailing edge of the wing (or the rotor plane of the helicopter), the spacing along the spray boom of the nozzle locations, and identification of nozzle type.

Drop size distributions are generally obtained from wind tunnel studies using a laser measuring instrument, with distributions recovered into 32 size classes. The Spray Drift Task Force measurements include component percentages, nozzle type, geometry, orientation, flow rate, pressure, and tunnel speed and have been collected in the AgDRIFT drop size distribution library. Alternately, the distribution may be estimated from empirical interpolation of the data [31,32].

Spray material characteristics include the flow rate, specific gravity, nonvolatile fraction (that portion of the tank mix that will not evaporate), active fraction (that portion of the tank mix that constitutes the nonvolatile active ingredients), and evaporation rate of the tank mix. These characteristics have been collected for many test substances in the AgDRIFT spray material library. Meteorological characteristics include wind speed, wind direction, temperature, and relative humidity, representing the layer where spray release and drift occur. AgDRIFT uses meteorological averages representative of the spraying time and a lag to cover atmospheric transport.

Meteorological data should be spatially representative of the modeling domain and averaged to recover representative data over the spray period for wind speed and wind direction [71] and for temperature and relative humidity. Estimates of the surface roughness parameter are also needed to compute wind speed profiles that are assumed logarithmic. AgDRIFT uses an evaporation model that requires the wet bulb temperature depression as input, collapsing temperature and relative humidity effects with the Carrier equation [47].

Other inputs into the model include the spraying height, the number of swaths flown across the spray block, swath width, and swath displacement (distance between the farthest downwind flight line and the edge of the field).

All model inputs are further constrained by sensible lower and upper limits, beyond which validation of model performance was not possible or degradation of model predictions would occur. These limits are summarized in Table 1 for tier II and tier III operation (units may be specified in English or metric in the program). Users are warned when these limits are exceeded.

MODEL FEATURES

For the assessment of aerial application, AgDRIFT computes the downwind drift and deposition of pesticides and the magnitude of buffer zones needed to protect sensitive aquatic and terrestrial habitats from undesired exposures. The methodology includes a screening or tier I level designed to yield conservative exposure estimates for downwind deposition and detailed or tier II and tier III levels requiring more knowledge of spraying conditions and information related to the specific spray material anticipated, spray system, and meteorological conditions. Tier I methodology is designed as a preliminary screen, based on user selection of one of the American Society of Agricultural Engineers Standard S-572 drop size distributions, patterned after the British Crop Protection Council categories of fine, medium, coarse, and very coarse [72–74]; tiers II and III permit increasing access to more model details.

The tier I aerial analysis is entered with the spray quality or atomization spectrum of the nozzle emission, the primary controlling variable for off-target drift. In tier I, the user can

Table 1. AgDRIFT® model limits[a]

Variable name	Tier II limits		Tier III limits	
	Lower	Upper	Lower	Upper
Active fraction	0.0001	nonvolatile fraction		
Boom height (m)	0.9	9.1	0.3	91.4
Boom length (%)	0.0	85.0	0.0	125.0
Surface roughness (m)			0.001	1.0
Flux plane (m)	0.0	304.0	0.0	792.0
Nonvolatile fraction	active fraction	1.0		
Number of flight lines	1	20	1	50
Relative humidity (%)	5.0	100.0	1.0	100.0
Spray rate (L/ha)	2.34	140.32	0.47	935.5
Swath displacement	−½ swath	2 swaths	−½ swath	10 swaths
Swath width (m)	4.6	30.4	3.1	152.4
Temperature (°C)	0.0	51.6		
Wind speed (m/s)	0.5	8.9	0.3	17.8
Wind direction (°)			−30.0	−150.0
Flying speed (m/s)	17.9	105.0	4.5	156.4
Nozzle orientation (°)[b]	0.0	90.0	0.0	150.0
Pressure (bar)	0.7	8.2	0.2	24.8

[a] Tier II surface roughness is 0.0076 m, wind direction is −90.0°.
[b] A nozzle orientation of 0° is straight back; 90° is straight down.

evaluate the upper limit of exposure and the effect of buffer zones assuming the generic labeling condition for the spray application. If spray quality and equipment usage to achieve this quality are specified on the label as well, the user can perform this analysis using the appropriate spray category rather than the default. If the estimated environmental exposure in tier I, coupled with the product toxicity for the organisms of concern, provides an adequate safety margin with the indicated buffer zone, then no additional analysis would be required. The assumptions used in the generation of the tier I aerial curves (Fig. 1) are consistent with the generic labeling language recommended by the U.S. Environmental Protection Agency's Office of Pesticide Programs for aerial spray applications.

If the user wishes to relax the generic label language restriction or reduce buffer zone requirements, then tier II may be appropriate. Tier II aerial analysis provides the mechanism to evaluate the effects on off-target drift of the most significant

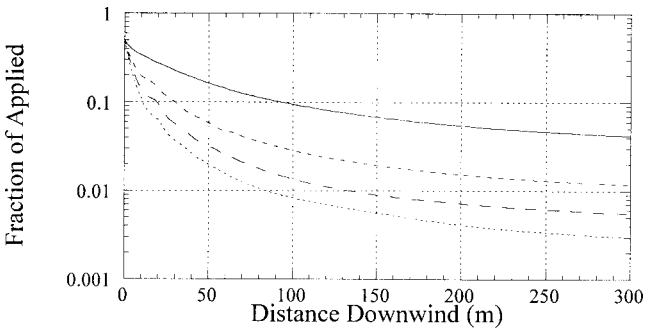

Fig. 1. Deposition as a function of distance for the four American Society of Agricultural Engineers Standard S-572 threshold categories. The 0-m location on the horizontal axis locates the edge of the field. These curves represent the upper range of deposition as a fraction of the nominal application rate when using recommended low-flight aerial labeling for fine (solid curve), medium (dashed curve), coarse (long dashed curve), and very coarse (dotted curve) atomization regimes. When no guidance is included on the label for spray quality, the fine to medium spray threshold should be used for spray application rates greater than 9.35 L/ha. Simulation results assume a 20-swath field application.

application and environmental variables. The specific variables that the user can evaluate in tier II include atomization spectra, wind speed, application area, temperature, relative humidity, aircraft class and speed, boom length, nonvolatile fraction, formulation properties, and release height above the canopy.

Tier III provides the analyst access to all aerial input variables and additional control of the variable limits. Generally, this tier is to be used to evaluate crop-, site-, formulation-, and equipment-specific applications. Likely uses include incident investigation, new application methods, special equipment specification, and unique site restrictions.

Model predictions are summarized in a numerical values section of the output. Typical plotted results available from AgDRIFT include incremental and cumulative drop size distribution, downwind deposition, average deposition (averaged over a defined pond width), flux/concentration through a vertical plane positioned downwind, swath width and mean deposition variation within the spray block as a function of coefficient of variation, and fraction aloft downwind. These results are described in the user manual [75]. The average (or pond-integrated) deposition is shown in Figure 2.

Tier II and tier III aerial predictions can be used to relax many of the tier I aerial assumptions and may be used to explore detailed model comparisons with data, parametric sensitivity in specific situations, or unique spraying scenarios. Contained within these tiers are various libraries and databases (containing information on aircraft, drop size distributions, and spray material physical properties), toolbox items (assessing the environmental consequences of the predicted scenario), and graphical output (plotting all important results of the prediction). A summary of the features contained within AgDRIFT may be found in Appendix 2. The toolbox features include the following.

The aquatic assessment toolbox permits the definition of a water body (pond or wetland) and calculations pertaining to the loading to that water body by the current calculated deposition pattern. The pond-integrated deposition curve (or the deposition curve if user-defined water body is selected) is interrogated to recover results when one of five inputs is specified: distance to water body from edge of field defines the

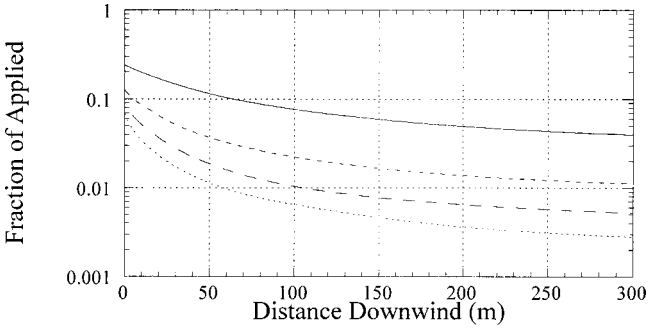

Fig. 2. Pond-integrated deposition as a function of distance for the four American Society of Agricultural Engineers Standard S-572 threshold categories. The 0-m location on the horizontal axis locates the edge of the field. These curves represent the upper range of pond-integrated deposition as a fraction of the nominal application rate when using recommended low flight aerial labeling for fine (solid curve), medium (dashed curve), coarse (long dashed curve), and very coarse (dotted curve) atomization regimes. Simulation results assume a 20-swath field application.

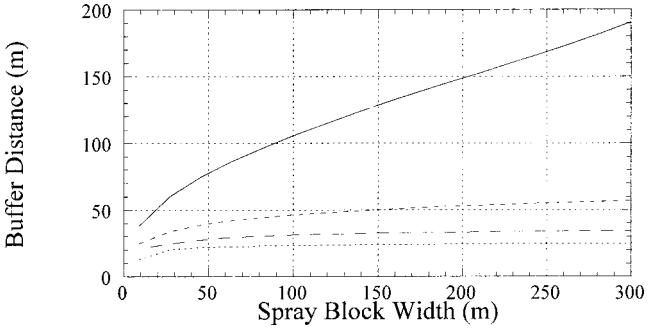

Fig. 3. Spray block assessment for the four American Society of Agricultural Engineers Standard S-572 threshold categories for deposition to a standard pond at a level of 0.05 fraction of applied. The 0-m location on the vertical axis locates the edge of the field. These curves represent the upper range of buffer distances needed for the spray block width flown to satisfy this application restriction for fine (solid curve), medium (dashed curve), coarse (long dashed curve), and very coarse (dotted curve) atomization regimes.

downwind distance; initial average deposition (of active spray material) recovers the average deposition across the width (downwind dimension) of the water body, in either fraction of applied, g/ha, or lb/acre; and initial average concentration (of active spray material) recovers the average concentration within the water body, in ng/L or ppt. Note that these average and integrated deposition and concentration estimates are based on the downwind deposition curve, with the deposition assumed uniform in the flight line direction.

The terrestrial assessment toolbox permits the definition of a surface area and calculations pertaining to the loading to that area by the current calculated point deposition pattern. The area average deposition curve (or the deposition curve if user-defined area average is selected) is interrogated to recover results when one of five inputs is specified: distance to point or area average from edge of field defines the downwind distance; and initial average deposition (of active spray material) recovers the average deposition across the width (downwind dimension) of the area, in either fraction of applied, g/ha, lb/acre, or mg/cm^2. Note that these average and integrated deposition estimates are again based on the downwind deposition curve, with the deposition assumed uniform in the flight line direction.

The drop distance toolbox accepts the inputs of drop size and release height and computes, with the Lagrangian solver, the drop size when the droplet hits the ground (evaporation effects), the distance traveled (wind speed effects), and the time to impact, with aircraft wake effects neglected.

The spray block statistics toolbox accepts the input of coefficient of variation of the deposit within the spray block, effective swath width, or mean deposition within the spray block and recovers the other two parameters from the appropriate curves. A coefficient of variation of 0.3 is suggested [76–78].

The spray block assessment toolbox permits an analysis of buffer distance as a function of spray block width. The assessment may be made in one of two modes, examining either the deposition pattern or the pond-integrated deposition pattern (conditioned by the water body description). In deposition mode, the user may specify the fraction of applied, g/ha, or lb/acre and recover the deposition level in the other units. This deposition level will generate a curve of spray block width (on the horizontal) and buffer distance to the specified deposition level (on the vertical). The buffer distance is measured from the edge of the field and is the distance to the desired deposition level, as a function of the width of the spray block (computed from the number of swaths and the swath width). The curve will always flatten as the spray block width increases because the far downwind deposition profile (and a consistent pond-integrated deposition profile) always shows decreasing deposition with increasing distance. The effect of adding spray lines deep within the spray block is therefore diminished. In pond-integrated deposition mode, the user may alternately specify the concentration in the stationary water body. Again, the desired pond-integrated deposition level will generate a curve of spray block width (on the horizontal) and buffer distance to the specified deposition level (on the vertical). A typical result is shown in Figure 3.

The stream assessment toolbox permits an analysis of the deposition to a stream located downwind of the spray block and the dispersion of that deposition as a function of time and distance downstream [67]. The characteristics of the stream and the application to the field are specified in the geometry section of the screen. The important, special stream parameters are the riparian interception factor (the fraction of material about to deposit in the stream but captured by vegetation just upwind of the stream [67]), the in-stream chemical decay rate (the time constant for the active ingredients to decay in water to one half their effectiveness [79]), and recharge rate (the amount of fresh water entering the stream downstream of the spray block [80]). In single-point mode, the stream assessment toolbox will return values at the point specified (in either time or distance). In distance range or time range mode, multiple curves will be generated. These curves represent the concentration profile in the stream at the times and distances selected and are an additive function of each of the flight lines depositing active spray material within the spray block. The plots become more disperse (spread out) as time or distance increases. The exposure analysis modeling system (EXAMS) button will generate a file of initial conditions for the time range option for input into that watershed model [81]. A typical result is shown in Figure 4.

The multiple application assessment toolbox permits an analysis of the multiple depositions to a field for more than a single event in a single year [82]. Multiple application assessment modifies the crosswind speed to recover variations

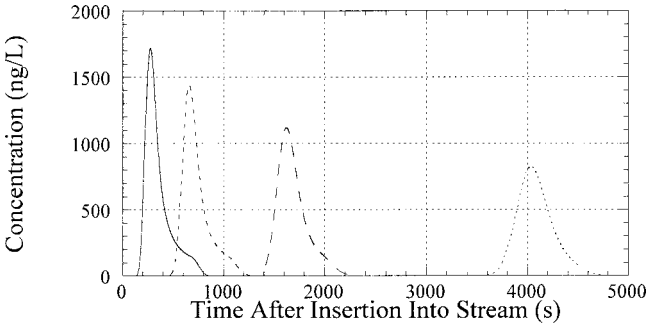

Fig. 4. Stream assessment for the fine to medium American Society of Agricultural Engineers Standard S-572 threshold category for dispersion to a stream for program defaults and a turnaround time of 20 s. Each of the four curves identifies a fixed distance downstream through which passes the concentration trace predicted here (solid curve for 251.2 m, dashed curve for 631.0 m, long dashed curve for 1,584.9 m, and dotted curve for 3,981.1 m).

in wind speed and direction for multiple events per year and multiple years (wind direction changes may be incorporated by a cosine correction to the wind speed). The characteristics of the wind speed and wind direction statistical profiles are entered (library data come from the Solar and Meteorological Surface Observational Network [SAMSON] database http://lwf.ncdc.noaa.gov/oa/ncdc.html) in the Wind Rose section. The user restricts the maximum wind speed to be examined and the months over which the events are to take place. The toolbox first generates the incremental wind speed deposition profiles needed for multiple application assessment, then runs controlled sampling to recover the specified wind speeds and wind directions. Summary deposition patterns may be plotted or the curve fits to the individual realizations may be exported to a file for later use by EXAMS. A typical result is shown in Figure 5.

MODEL LIMITATIONS

AgDRIFT limitations are primarily found in the extent of the physics on which the model is based and the extent of the field data against which the model has been evaluated. AgDRIFT is presently a near-field model that is applicable to the region in which the aircraft wake is expected to have influence over the behavior of the released spray material. Model

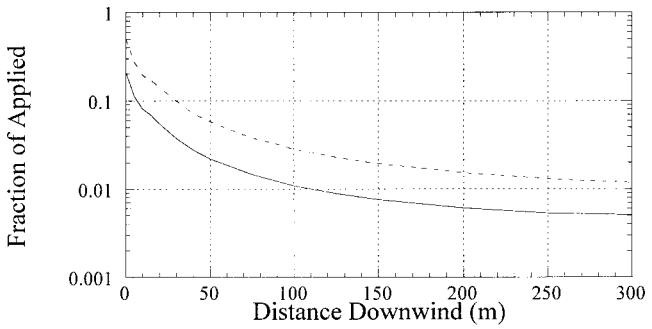

Fig. 5. Multiple application assessment for the fine to medium American Society of Agricultural Engineers Standard S-572 threshold category for Sioux City (IA, USA). The 0-m location on the horizontal axis locates the edge of the field. The two curves shown are the average multiple application deposition pattern (solid curve, including zero deposition effects when the wind is blowing upwind of the spray block) and the maximum deposition pattern recovered across the wind speed range selected (dashed curve). Ten events per year for 10 years were assumed in this example.

validation [40] compares model predictions to 800 m, and in a strict sense limits buffer distances to 800 m as well, although model predictions may be extended to nearly 1,600 m in tier III. The applicability of the Lagrangian model to the problem of aerial spraying may be further investigated by examining three time scales involved in drift as it is defined here [83].

Vortex decay

Near-field drift is considered near-field because of the influence of the aircraft wake. It is therefore important to estimate the time scale for decay of the aircraft-generated vortices by atmospheric turbulence. For convenience, we examine the wake of an AgHusky, an aircraft used in the Spray Drift Task Force field trials [84]. The vortex decay rate was quantified in an extensive set of field studies with anemometer tower grids recording the passage of descending aircraft vortices [58] and is given by Equation 39. When the argument in the exponential of Equation 39 reaches -6, the vortex strength has decayed to 0.0025 of its initial value. Thus, the vorticity may be considered to have dissipated to the point where it would no longer be influencing the motion of the released spray material. For the AgHusky, this argument corresponds to a time of influence of the vortices of 68 s. For a typical crosswind of 4.47 m/s (the tier I default wind speed), these numbers suggest that aircraft vortices will influence the behavior of the released spray out to 300 m downwind (the downwind extent in tiers I and II). Such a distance is reasonably well within (and beyond) the size of buffer zones typically imposed in agricultural applications and supports the use of the Lagrangian solution technique for near-field drift prediction.

Vortex bounce

While the vortices are descending to the surface, they cause viscous forces within the boundary layer to form countersign vorticity to oppose their motion. This effect has been modeled by Bilanin et al. [85], who show that the ground begins to influence the behavior of vortices by a nondimensional time of $t\Gamma/2\pi s^2 = 8$. Again, for the AgHusky, the time is computed to be 79 s. It may be seen, then, that vortex bounce effects will not begin to be important until well past most buffer zones. Also, although the explicit effects of vortex bounce have not been programmed into the Lagrangian model, parameterizing the effect of vortex decay is probably capturing some of the physics of the bounce.

Evaporation

The third effect that influences the near-field model is that of droplet evaporation. A detailed study of pesticide tank mix evaporation rates [49] along with data interpretation [50] show that evaporation typically occurs within a time scale of $t\Delta\Theta Sh/2D^2 = 0.01$. For example, conditions of a temperature of 15.5°C, relative humidity of 60%, and a drop diameter of 100 μm, the time for evaporation is computed to be 24 s. This time is relatively short for a wide range of conditions and drop sizes, suggesting that evaporation is an important part of the near-field solution.

These three separate effects play an important role in the solution for the primary drift effects caused by the aircraft wake and its influence on the released spray material. The assumption of elliptical wing loading, vortex decay, simple water-like evaporation, and use of wind-tunnel-determined drop size distributions and consistent meteorological conditions all lead to an accurate prediction of the deposition ex-

pected from the aerial application of spray materials. These scales are important for modeling near-field drift, and encompassing most buffer zones around sensitive areas.

Beyond near-field, other physical effects come into play that are considered (at present) beyond the scope of the AgDRIFT model or that lead to a breakdown in the assumptions made to generate the model. These include atmospheric stability (although efforts [86] are on-going to expand beyond the neutral atmosphere assumption), terrain and mesoscale effects, including time-dependent meteorology (the current model assumes a flat earth and steady-state ambient conditions), point vortex limitations (especially in the so-called upwind-downwind vortex location problem [87]), and limitations on the applicability of drop size distributions generated in the wind tunnel (especially for straight stream nozzles as discussed in [40]).

SUMMARY

This article has summarized the development and implementation of AgDRIFT, an extension of the original AGDISP Lagrangian model for the prediction of downwind drift and deposition from the aerial application of spray materials. The applicability of the Lagrangian trajectory analysis, the drop size distribution data, evaporation modeling, fixed-wing and helicopter models, vortex decay effects, and consistent ground deposition models are all supported by model comparisons with field data. These comparisons present a powerful argument for the applicability of AgDRIFT in predicting the downwind deposition and drift of aerially released spray material.

Acknowledgement—Development of AGDISP could not have taken place without the support of Robert B. Ekblad and John W. Barry. Refinement of AGDISP into AgDRIFT could not have been accomplished without the guidance of the Spray Drift Task Force Modeling Subcommittee and the support and data-gathering commitment of the Spray Drift Task Force. This article has been reviewed in accordance with the U.S. Environmental Protection Agency and National Oceanic and Atmospheric Administration peer and administrative review policies and has been approved for publication. Mention of trade names or commercial products does not constitute endorsement or recommendation for use by the U.S. Environmental Protection Agency or the National Oceanic and Atmospheric Administration.

REFERENCES

1. Hewitt AJ, Johnson DR, Fish JD, Hermansky CG, Valcore DL. 2002. Development of the Spray Drift Task Force database for aerial applications. *Environ Toxicol Chem* 21:648–658.
2. Crabbe RS, McCooeye MA, Mickle RE. 1994. The influence of atmospheric stability on wind drift from ultra-low-volume aerial forest spray applications. *J Appl Meteorol* 33:500–507.
3. Maybank J, Yoshida K, Grover R. 1978. Spray drift from agricultural pesticide applications. *J Air Pollut Control Assoc* 28: 1009–1014.
4. Yates WE, Akesson NB, Cowden RE. 1974. Criteria for minimizing drift residues on crops downwind from aerial applications. *Trans ASAE* 17:627–632.
5. Yates WE, Akesson NB, Coutts HH. 1966. Evaluation of drift residues from aerial applications. *Trans ASAE* 9:389–393.
6. Yates WE, Akesson NB, Coutts HH. 1967. Drift hazards related to ultra-low-volume and dilute sprays by agricultural aircraft. *Trans ASAE* 10:628–632, 638.
7. Ware GW, Cahill WP, Estesen BJ. 1974. Pesticide drift: Aerial applications comparing conventional flooding vs. raindrop nozzles. *J Econ Entomol* 68:329–330.
8. Bird SL, Esterly DM, Perry SG. 1996. Off-target deposition of pesticides from agricultural aerial spray applications. *J Environ Qual* 25:1095–1104.
9. Himel CM, Loats H, Bailey GW. 1990. Pesticide sources to the soil and principles of spray physics. In *Pesticides in the Soil Environment*. SSSA Book Series 2. Soil Science Society of America, Madison, WI, pp 7–50.
10. Saputro S, Smith DB. 1990. Expert system for aerial spray drift. Paper 90-1018. American Society of Agricultural Engineers, Columbus, OH.
11. Bache DH, Sayer WJD. 1975. Transport of aerial spray I: A model of aerial dispersion. *Agric Meteorol* 15:257–271.
12. Bilanin AJ, Teske ME, Barry JW, Ekblad RB. 1989. AGDISP: The aircraft spray dispersion model, code development and experimental validation. *Trans ASAE* 32:327–334.
13. Gaidos RE, Patel MR, Valcore DL, Fears RD. 1990. Prediction of spray drift deposition from aerial applications of pesticides. Paper AA90-007. National Association of Aerial Applicators/ American Society of Agricultural Engineers Joint Technical Session, Reno, NV, USA.
14. Teske ME, Bowers JF, Rafferty JE, Barry JW. 1993. FSCBG: An aerial spray dispersion model for predicting the fate of released material behind aircraft. *Environ Toxicol Chem* 12:453–464.
15. Wallace DJ, Picot JJC, Chapman TJ. 1995. A numerical model for forestry aerial spraying. *Agric For Meteorol* 76:19–40.
16. Dumbauld RK, Bjorklund JR. 1977. Mixing-layer analysis routine and transport/diffusion application routine for EPAMS. ECOM-77-2. Technical Report. Atmospheric Sciences Laboratory, U.S. Army Electronics Command, White Sands Missile Range, NM.
17. Dumbauld RK, Bjorklund JR, Saterlie SF. 1980. Computer models for predicting aircraft spray dispersion and deposition above and within forest canopies: User's manual for the FSCBG computer program. Report 80-11. U.S. Department of Agriculture Forest Service, Davis, CA.
18. Frost W, Huang KH. 1981. Monte Carlo model for aircraft applications of pesticides. Paper 81-1507. American Society of Agricultural Engineers, Chicago, IL.
19. Teske ME, Barry JW, Thistle HW. 1994. Aerial spray drift modeling. In Zannetti P, ed, *Environmental Modeling*, Vol 2—Computer Methods and Software for Simulating Environmental Pollution and Its Adverse Effects. Computational Mechanics Publications, Southampton, UK, pp 11–42.
20. Reed WH. 1953. An analytical study of the effect of airplane wake on the lateral dispersion of aerial sprays. Report 3032. National Advisory Committee for Aeronautics, Langley, VA, USA.
21. Williamson RB, Threadgill ED. 1974. A simulation for the dynamics of evaporating spray droplets in agricultural spraying. *Trans ASAE* 17:254–261.
22. Trayford RS, Welch LW. 1977. Aerial spraying: A simulation of factors influencing the distribution and recovery of liquid droplets. *J Agric Eng Res* 22:183–196.
23. Atias M, Weihs D. 1984. Motion of aircraft trailing vortices near the ground. *J Aircraft* 21:783–786.
24. Bragg MB. 1986. A numerical simulation of the dispersal of liquid from aircraft. *Trans ASAE* 29:10–15.
25. Bilanin AJ, Teske ME. 1984. Numerical studies of the deposition of material released from fixed and rotary wing aircraft. NASA CR 3779. National Aeronautics and Space Administration, Langley, VA, USA.
26. Hardy CE. 1987. Aerial application equipment. Report 8734-2804. U.S. Department of Agriculture Forest Service, Missoula, MT.
27. MacNichol AZ. 1993. Spray Drift Task Force aircraft sensitivity study. Technical Note 93-20. Continuum Dynamics, Ewing, NJ, USA.
28. Hewitt AJ. 1995. Spray Drift Task Force atomization droplet size spectra for selected active ingredients. Study A92-004, EPA MRID 43766502. U.S. Environmental Protection Agency, Office of Pesticide Programs, Washington, DC.
29. Hewitt AJ. 1996. Spray Drift Task Force atomization droplet size spectra for nozzle and physical property parameter characterization. Study A92-003, EPA MRID 44100901. U.S. Environmental Protection Agency, Office of Pesticide Programs, Washington, DC.
30. Teske ME, Bilanin AJ. 1994. Drop size scaling analysis of non-Newtonian fluids. *Atomization and Sprays* 4:473–483.
31. Hermansky CG, Hewitt AJ, Johnson DR. 1997. Relationship between physical properties and atomization: Integration and summary. MRID 44747401. U.S. Environmental Protection Agency, Office of Pesticide Programs, Washington, DC.
32. Esterly DM. 1998. Neural network analysis of Spray Drift Task

Force atomization DropKick® II. Paper 981014. American Society of Agricultural Engineers, Orlando, FL.
33. Teske ME, Thistle HW. 2000. Droplet size scaling of agricultural spray material by dimensional analysis. *Atomization and Sprays* 10:147–158.
34. Teske ME. 1992. Spray Drift Task Force model comparison. Technical Note 92-01. Continuum Dynamics, Ewing, NJ, USA.
35. Teske ME, Barry JW. 1993. Parametric sensitivity in aerial application. *Trans ASAE* 36:27–33.
36. Teske ME. 1996. Evaluation of the FSCBG aerial spray model's near-wake sensitivity to selected input parameters. Report FHTET 96-30. U.S. Department of Agriculture Forest Service, Davis, CA.
37. Teske ME, Thistle HW, Barry JW, Eav B. 1998. A simulation of boom length effects for drift minimization. *Trans ASAE* 41:545–551.
38. Teske ME, Thistle HW. 1999. A simulation of release height and wind speed effects for drift minimization. *Trans ASAE* 42:583–591.
39. Teske ME, Thistle HW, Eav B. 1998. New ways to predict aerial spray deposition and drift. *J For* 96:25–31.
40. Bird SL, Perry SG, Ray SL, Teske ME. 2002. Evaluation of the AgDISP aerial spray algorithms in the AgDRIFT model. *Environ Toxicol Chem* 21:672–681.
41. Langmuir I, Blodgett KB. 1949. A mathematical investigation of water droplet trajectories. Report RL225. General Electric, Schenectady, NY, USA.
42. Tennekes H, Lumley JL. 1972. *A First Course in Turbulence.* MIT Press, Cambridge, MA, USA.
43. von Karman TD, Howarth L. 1938. On the statistical theory of isotropic turbulence. *Proc R Soc Lond A* 164:192–215.
44. Houbolt JC, Steiner R, Pratt KG. 1964. Dynamic response of airplanes to atmospheric turbulence including flight data on input and response. NASA TR R-199. National Aeronautics and Space Administration, Langley, VA, USA.
45. Lewellen WS, Teske ME. 1976. Second-order closure modeling of diffusion in the atmospheric boundary layer. *Bound-Layer Meteorol* 10:60–90.
46. Monin AS, Yaglom AM. 1973. *Statistical Fluid Mechanics: Mechanics of Turbulence.* MIT Press, Cambridge, MA, USA.
47. Jennings BH, Lewis SR. 1950. *Air Conditioning and Refrigeration.* International Textbook, Scranton, PA, USA.
48. Meyer CA, McClintock RB, Silvestri GJ, Spencer RC. 1979. *ASME Steam Tables—Thermodynamic and Transport Properties of Steam,* 4th ed. American Society of Mechanical Engineers, New York, NY.
49. Riley CM, Sears II, Picot JJC, Chapman TJ. 1995. Spray Drift Task Force droplet evaporation studies. In Hall FR, Berger PD, Collins HM, eds, *Pesticide Formulations and Application Systems,* Vol 14. STP 1234. American Society for Testing and Materials, Philadelphia, PA, pp 225–236.
50. Teske ME, Hill RL. 1995. The evaporation rate of agricultural spray material. *Proceedings,* Institute for Liquid Atomization and Spray Systems Americas 8th Annual Conference on Liquid Atomization and Spray Systems, Troy, MI, USA, pp 19–23.
51. Fuchs NA. 1959. *Evaporation and Droplet Growth in Gaseous Media.* Pergamon, Elmsford, NY, USA.
52. Teske ME, MacNichol AZ. 1996. An interpretation of the RPC evaporation data. Technical Note 94-05. Continuum Dynamics, Ewing, NJ, USA.
53. Teske ME, Hermansky CG, Riley CM. 1998. Evaporation rates of agricultural spray material at low relative wind speeds. *Atomization and Sprays* 8:471–478.
54. Donaldson CduP, Bilanin AJ. 1975. Vortex wakes of conventional aircraft. AGARD-AG-204. North Atlantic Treaty Organization, Advisory Group for Aerospace Research and Development, Technical Editing and Reproduction, London, UK.
55. Bilanin AJ, Teske ME. 1994. Aircraft wake and droplet dispersion. Technical Memo 94-03. Continuum Dynamics, Ewing, NJ, USA.
56. Kuethe AM, Schetzer JD. 1959. *Foundations of Aerodynamics.* John Wiley, New York, NY, USA.
57. Lewellen WS, Teske ME, Donaldson CduP. 1974. Application of turbulence model equations to axisymmetric wakes. *Am Inst Aeronautics Astronautics J* 12:620–625.
58. Teske ME, Bilanin AJ, Barry JW. 1993. Decay of aircraft vortices near the ground. *Am Inst Aeronautics Astronautics J* 31:1531–1533.
59. Bramwell ARS. 1976. *Helicopter Dynamics.* John Wiley, New York, NY, USA.
60. Wachspress DA, Quackenbush TR, Boschitsch AH, Lam CMG. 1996. *RotorCRAFT/AA (mod 1.0) User's Manual.* Technical Note 95-23. Continuum Dynamics, Ewing, NJ, USA.
61. Schlicting H. 1968. *Boundary Layer Theory,* 7th ed. McGraw-Hill, New York, NY, USA.
62. Wygnanski I, Fiedler H. 1969. Some measurements in the self-preserving jet. *J Fluid Mechanics* 38:577–612.
63. Donaldson CduP. 1973. Atmospheric turbulence and the dispersal of atmospheric pollutants. In Haugen DA, ed, *AMS Workshop on Micrometeorology.* Science Press, Boston, MA, USA, pp 313–390.
64. Lewellen WS. 1977. Use of invariant modeling. In Frost W, Moulden TH, eds, *Handbook of Turbulence.* Plenum, New York, NY, USA, pp 237–280.
65. Fischer HB, List EJ, Koh RCY, Imberger J, Brooks NH. 1979. *Mixing in Inland and Coastal Waters.* Academic, San Diego, CA, USA.
66. Carslaw HS, Jaeger JC. 1959. *Conduction of Heat in Solids,* 2nd ed. Oxford University Press, London, UK.
67. Teske ME. 2000. Stream modeling assessment with AgDRIFT®. Technical Bulletin 808. National Council of the Paper Industry for Air and Stream Improvement, Research Triangle Park, NC, USA.
68. Teske ME. 1989. An examination of AGDISP helicopter model comparisons with data and detailed helicopter code predictions. Technical Note 89-01. Continuum Dynamics, Ewing, NJ, USA.
69. Teske ME, Barry JW. 1993. FSCBG spray drift predictions. Paper 931101. American Society of Agricultural Engineers, Spokane, WA.
70. Lambert M, ed. 1992. *Jane's All the World's Aircraft.* Jane's Publishing, New York, NY, USA.
71. Haugen DA. 1963. A simplified method for automatic computation of turbulent wind direction statistics. *J Appl Meteorol* 2: 306–308.
72. Doble SJ, Matthews GA, Rutherford I, Southcombe ESE. 1985. A system for classifying hydraulic nozzles and other atomisers into categories of spray quality. *Proceedings,* British Crop Protection Conference, Vol 3, Brighton, UK, pp 1125–1133.
73. Southcombe ESE. 1988. The BCPC nozzle selection system. *Proceedings,* International Symposium on Pesticide Applications, Paris, France, pp 71–78.
74. Parkin CS, Gilbert AJ, Southcombe ESE, Marshall CJ. 1994. British Crop Protection Council scheme for the classification of pesticide application equipment by hazard. *Crop Prot* 13:281–285.
75. Teske ME, Bird SL, Esterly DM, Ray SL, Perry SG. 2001. A user's guide for AgDRIFT® 2.0: A tiered approach for the assessment of spray drift of pesticides. Report 01-01. Continuum Dynamics, Ewing, NJ, USA.
76. Parkin CS, Wyatt JC. 1982. The determination of flight-line separations for the aerial application of herbicides. *Crop Prot* 1:309–321.
77. Quantick HR. 1985. *Aviation in Crop Protection, Pollution and Insect Control.* Collins, London, UK.
78. Teske ME, Twardus DB, Ekblad RB. 1990. Swath width evaluations. Report 9034-2807-MTDC. U.S. Department of Agriculture Forest Service, Missoula, MT.
79. Hornsby AG, Wauchope RD, Herner AE. 1996. *Pesticide Properties in the Environment.* Springer-Verlag, New York, NY, USA.
80. Lahlou M, Shoemaker L, Paquette M, Bo J, Choudhury S, Elmer R, Xia F. 1996. *Better Assessment Science Integrating Point and Nonpoint Sources: BASINS User's Manual,* Ver 1.0. EPA-823-R-96-001. Office of Science and Technology, U.S. Environmental Protection Agency, Washington, DC.
81. Burns LA. 1997. *Exposure Analysis Modeling System (EXAMS II): User's Guide,* Ver 2.97.5. EPA/600/R-97/047. Office of Research and Development, U.S. Environmental Protection Agency, Athens, GA.
82. Teske ME. 2000. Multiple application assessment in AgDRIFT® 2.0. Technical Note 00-02. Continuum Dynamics, Ewing, NJ, USA.
83. Teske ME. 1998. Droplet dispersion by Lagrangian methods. *Proceedings,* Institute for Liquid Atomization and Spray Systems Americas 11th Annual Conference on Liquid Atomization and Spray Systems, Sacramento, CA, USA, pp 303–307.

84. Johnson DR. 1995. Drift from applications with aerial sprayers: Integration and summary of 1992 and 1993 field studies. Study I94-002. EPA MRID 43803501. U.S. Environmental Protection Agency, Office of Pesticide Programs, Washington, DC.
85. Bilanin AJ, Teske ME, Hirsh JE. 1978. Neutral atmospheric effects on the dissipation of aircraft vortex wakes. *Am Inst Aeronautics Astronautics J* 16:956–961.
86. Thistle HW, Teske ME, Barry JW. 1996. Incorporation of stability effects into a Lagrangian subroutine used to model wake and ambient dispersion in the atmosphere. *Proceedings*, American Meteorological Society 9th Conference on Applications of Air Pollution Meteorology, Atlanta, GA, USA, pp 538–541.
87. Teske ME, Thistle HW, Mickle RE. 1998. Detailed model simulations behind fixed-wing agricultural aircraft. Paper 981022. American Society of Agricultural Engineers, Orlando, FL.

APPENDIX 1

AgDRIFT® input summary

- Aircraft information
  - Aircraft type (fixed-wing, biplane, helicopter)
  - Aircraft semispan or rotor radius
  - Spraying speed
  - Rotor blade RPM (helicopter)
  - Aircraft weight
- Propeller information
  - Aircraft drag coefficient
  - Aircraft platform area
  - Engine efficiency
  - Propeller RPM
  - Propeller blade radius
  - Propeller location
- Nozzle information
  - Number of nozzles
  - Nozzle type
  - Nozzle locations
- Drop size distribution
- Spray material information
  - Tank mix specific gravity
  - Tank mix flow rate
  - Tank mix nonvolatile fraction
  - Tank mix active fraction
  - Evaporation rate
- Meteorological information
  - Wind speed
  - Height of wind speed measurement
  - Surface roughness
  - Wind direction
  - Wet bulb temperature depression (temperature and relative humidity)
- Other information
  - Spraying height
  - Number of swaths
  - Swath width
  - Swath displacement

APPENDIX 2

Summary of features available in AgDRIFT®

- Model inputs
  - Active rate
  - Aircraft
  - Boom height
  - Boom length
  - Drop size distribution
  - Evaporation rate
  - Flux plane location
  - Nonvolatile rate
  - Number of flight lines
  - Relative humidity
  - Specific gravity
  - Spray rate
  - Surface roughness
  - Swath displacement
  - Swath width
  - Temperature
  - Wind direction
  - Wind speed
- Libraries

Drop size distribution	1,294 entries
Nozzle characteristics	59 entries
Spray material properties	122 entries
Evaporation properties	68 entries
Aircraft description	72 entries

- Graphical output
  - Drop size distribution: initial, downwind, vertical profile
  - Deposition
  - Pond-integrated deposition
  - Vertical profile
  - 1-h average concentration
  - Coefficient of variation
  - Mean deposition
  - Fraction aloft
- Toolboxes
  - Aquatic assessment
  - Terrestrial assessment
  - Drop distance
  - Spray block statistics
  - Spray block assessment
  - Stream assessment
  - Multiple application assessment